Defect prevention in silica thin films synthesized using AP-PECVD for flexible electronic encapsulation

Fiona M Elam[1-3], Sergey A Starostin[1], Anna S Meshkova[2,3], Bernadette C A M van der Velden-Schuermans[1], Mauritius C M van de Sanden[2,3] and Hindrik W de Vries[3]

[1]FUJIFILM Manufacturing Europe B.V., P.O. Box 90156, 5000 LJ Tilburg, The Netherlands.
[2]Eindhoven University of Technology, Applied Physics, P.O. Box 513, 5600 MB Eindhoven, The Netherlands.
[3]DIFFER – Dutch Institute for Fundamental Energy Research, P.O. Box 6336, 5600 HH Eindhoven, The Netherlands.

E-mail: f.m.elam@differ.nl

Abstract. Industrially and commercially relevant roll-to-roll atmospheric pressure-plasma enhanced chemical vapour deposition was used to synthesize smooth, 80 nm silica-like bilayer thin films comprising a dense 'barrier layer' and comparatively porous 'buffer layer' onto a flexible polyethylene 2,6 naphthalate substrate. For both layers, tetraethyl orthosilicate was used as the precursor gas, together with a mixture of nitrogen, oxygen and argon. The bilayer films demonstrated exceptionally low effective water vapour transmission rates in the region of 6.1×10^{-4} g m^{-2} day^{-1} (at 40°C, 90% relative humidity), thus capable of protecting flexible photovoltaics and thin film transistors from degradation caused by oxygen and water. The presence of the buffer layer within the bilayer architecture was mandatory in order to achieve the excellent encapsulation performance. Atomic force microscopy in addition to solvent permeation measurements, confirmed that the buffer layer prevented the formation of performance-limiting defects in the bilayer thin films, which likely occur as a result of excessive plasma-surface interactions during the deposition process. It emerged that the primary function of the buffer layer was therefore to act as a protective coating for the flexible polymer substrate material.

1. Introduction

Encapsulation films, typically consisting of single or multilayer stacks of silicon nitride, alumina, silica or titania [1–23], are essential to the flexible electronics industry, envisioned to protect devices such as flexible solar cells, thin film transistors, quantum dot liquid crystal displays and organic light emitting diodes (OLEDs) against degradation from oxygen and water [1–8].

It is known that single layer encapsulation performance is limited by the presence of defects, such as cracks or pinholes in the inorganic layer [1–4,9,24,25]. Studies have shown that the use of multilayer encapsulation barriers [1,3–7,10–12,24], deposited using techniques such as sputtering, atomic layer deposition and molecular layer deposition processes, can prevent the formation [1,3–5], and propagation [3], of such defects. Water vapour transmission rate (WVTR) values for multilayer encapsulation barriers have been reported within the region of 10^{-5} g m^{-2} day^{-1} (at 30°C, 90% relative

humidity (RH)) [1,6,7], and hence almost achieve the OLED protection requirement of 1×10^{-6} g m^{-2} day^{-1} (at 25°C, 40% RH) [4,5,8,12].

However, cost effective manufacturing of encapsulation films is crucial, and the generation of the aforementioned multilayer barriers can be highly expensive due to the alternate vacuum deposition processes usually required for their synthesis [3]. Processes performed at atmospheric pressure, such as atmospheric pressure-plasma enhanced chemical vapour deposition (AP-PECVD), therefore present a significantly more favourable solution [3,9,26,27].

Roll-to-roll AP-PECVD was recently used to produce smooth, 90 nm silica-like bilayer thin films comprising a dense inorganic 'barrier layer' and comparatively porous inorganic 'buffer layer' that demonstrated exceptionally good encapsulation performance with effective water vapour transmission rates in the region of 6.9×10^{-4} g m^{-2} day^{-1} (at 40°C, 90% RH) [26]. Despite this value not quite being low enough to meet the WVTR requirement for flexible OLEDs [4,5,8,12], it was however the lowest effective WVTR obtained to date for a silica-like film deposited upon a flexible polymer substrate by AP-PECVD, and suitable for the protection of flexible photovoltaics and thin film transistors [3,4,28]. By using the same material in the multilayer film architecture, and by having AP-PECVD as the deposition method, rendered this investigation highly industrially and commercially relevant to the eventual large scale production of flexible encapsulation foils. It was discovered that increasing the input energy per precursor gas molecule during the deposition of the dense barrier layer, resulted in an improved encapsulation performance. Nevertheless, the individual role performed by each layer in the overall success of the bilayer films is not yet fully understood.

The use of an organic 'buffer layer' was previously found to be responsible for the improved adhesion of 'high barrier' silica-like coatings deposited onto polyethylene terephthalate substrates by pulsed low-pressure microwave plasmas [29]. However, it is unlikely in the case of the aforementioned silica-like bilayer films that the purpose of the inorganic porous buffer layer is merely to promote adhesion. The focus of the presented work is therefore to understand the function of the porous buffer layer in a bilayer silica-like encapsulation film deposited using roll-to-roll AP-PECVD. A deeper insight into the necessity for such a layer in an encapsulation film, will further efforts to improve both film quality and process throughput, making roll-to-roll AP-PECVD processing commercially accessible.

2. Experimental

A glow-like atmospheric pressure dielectric barrier discharge in a roll-to-roll set-up open to ambient air was used to synthesize 80 nm (81 ± 5 nm) silica-like bilayer films comprising a 30 nm (32 ± 2 nm) barrier layer deposited over a 50 nm (49 ± 5 nm) buffer layer; and 65 nm (64 ± 4 nm) silica-like bilayer films comprising a 15 nm (16 ± 2 nm) barrier layer deposited over a 50 nm (48 ± 3 nm) buffer layer by PECVD. Similarly, 30 nm (27 ± 4 nm) and 15 nm (16 ± 3 nm) single layer barrier films were deposited so that the function of the ~50 nm buffer layer with regard to the bilayer encapsulation performance could be evaluated. A schematic representation of the AP-PECVD reactor is shown in [9], and basic device and thin film deposition parameters can be found in a recent publication by Elam et al. [26]. The reactor is located in an ISO class 3 cleanroom, in accordance with ISO 14644-1 standards.

Thermally stabilized optical grade polyethylene 2,6 naphthalate (PEN) foil (Teonex Q65HA, Teijin DuPont Films) with a width and depth of 180 mm and 100 μm respectively, was positioned over the lower drum electrode and thus acted as the substrate material. A 63 μm thick sacrificial polymer, polyethylene terephthalate (PET) (ASTERA Functional Foils, AGFA), was used as the dielectric material for the upper drum electrode. The PEN foil transport speed was fixed at 400 mm min^{-1} to ensure a 50 nm deposition during the buffer layer synthesis, varied from 372 – 35 mm min^{-1} to enable the deposition of a ~30 nm barrier, and adjusted from 744 – 80 mm min^{-1} to guarantee that a ~15 nm barrier layer was deposited. In all cases, the sacrificial upper PET foil transport speed was maintained at 50 mm min^{-1}.

The reactant gases in each case were oxygen (technical grade) and tetraethyl orthosilicate (Si(OC$_2$H$_5$)$_4$, TEOS) (≥99.0%, Sigma-Aldrich). The precursor gas, TEOS, was injected via a controlled evaporation mixer unit (CEM-Technology, Bronkhorst HIGH-TECH B.V.), where the

vapours were combined with 1 slm argon (technical grade). The carrier gas in all cases was nitrogen (technical grade), with a flow of 15 slm for buffer layer synthesis and 20 slm for barrier layer synthesis. All four gases were combined in the gas injector before being released into the plasma. The reactant gas flows for buffer layers were kept constant at 8.3×10^{-3} slm TEOS and 1.8 slm oxygen, resulting in layers with a deposition input energy of 1.6 keV/TEOS molecule. However, in order to vary the input energy per TEOS molecule and therefore the layer densities [9,26], for both the 30 nm and 15 nm barrier layers, the TEOS and oxygen gas flows were adjusted with a fixed ratio of 4.5×10^{-3} in the range of $3.6 \times 10^{-3} - 0.2 \times 10^{-3}$ slm and $0.8 - 0.05$ slm respectively. This resulted in the deposition of barrier layers with input energies ranging from approximately $3 - 30$ keV/TEOS molecule. A description of the method used to calculate the input energy per TEOS molecule is outlined in a publication by Elam et al. [26]. It should be noted that because of system limitations, for films deposited with barrier layer oxygen gas flows below 0.075 slm, dry air was used as the reactant gas in place of oxygen.

Spectroscopic ellipsometry was performed using a variable angle spectroscopic ellipsometer (M-2000D, J.A. Woollam Co. Inc.) in the wavelength range of $400 - 1000$ nm in order to determine the thickness of the buffer layers, the combined buffer-barrier bilayers and the single layer barriers post-deposition. The Cauchy dispersion function was used to model the PEN substrate and the silica-like thin films as two separate entities. The optical model did not take into account the substrate anisotropy; however sample orientation was consistent for each measurement.

The effective WVTR of both bilayer samples comprising barrier, buffer and substrate layers, and single layer samples comprising barrier and substrate layers were determined using a Deltaperm (Technolox Ltd.), with set conditions of 40°C, 90% RH. This measurement therefore took into account the overall permeation of the films; including contributions from macro-defects (>1 nm), and the intrinsic microstructure (nano-defects ($0.3 - 1$ nm) and gas transport through the amorphous silica-like lattice itself ($0.2 - 0.3$ nm)) [30]. The Deltaperm is a direct pressure device that fulfils the ASTM D 1434-82 (2003) standard for permeation measurements, and has a WVTR limit of 2×10^{-4} g m^{-2} day^{-1}. Sample areas of 50 cm^2 were investigated, with each measurement lasting for $5 - 120$ hrs depending on encapsulation ability, in order to ensure the permeation rate had stabilized. The WVTR was recorded each minute, and calculated as summarized in [26].

The presence of any 'large' defects in the 30 nm single layer and bilayer films were determined by means of exposure to a solvent vapour for 1.5 hours and 24 hours respectively. The solvent had a molecular kinetic diameter of 0.33 nm, which enabled it to permeate through macro-defects and potentially also nano-defects in the silica layer [30], to the underlying PEN substrate. This resulted in the formation of circular blisters at the location of these defects due to the locally enhanced solubility of the solvent in the PEN substrate [31]. Interferometric microscopy (Wyko NT9100 Optical Profiling System, Veeco Instruments Inc.) was then carried out on the films post-exposure to detect for the presence of these blisters and hence for macro-defects in the silica-like films. The interferometric microscopy measurement was performed in phase-shift interferometry mode, analysing an area of 47×63 μm^2. Micrographs were then processed and stitched to form images with areas of 25 mm^2 using Wyko Vision software. The defect density (defect number per cm^2) was calculated from an average of 10 stitched interferometric micrographs, with circular peaks greater than 0.3 μm in height considered defects. In total, an area of 2.5 cm^2 was evaluated for every sample.

Atomic force microscopy (AFM) (Park NX10, Park Systems) was performed to investigate the surface morphology of the PEN substrate, the buffer layer, bilayer and single layer barriers. The measurements were implemented in tapping mode, using a tip with a radius of approximately 8 nm. Images of 512×512 pixels obtained with a scanning area of 2×2 μm^2, were then processed using Gwyddion software in order to obtain root mean square (RMS) roughness values of the layers [32].

3. Results and discussion

Figure 1 shows the effective WVTR trend (at 40°C, 90% RH) with respect to increasing input energy per TEOS precursor molecule (a parameter that relates increasing plasma residence time with decreasing TEOS vapour flow rates, whilst maintaining a constant power dissipation in the discharge) during the deposition of the barrier layer for four different film types. At input energies of 3

keV/TEOS molecule, the presence of a buffer layer appears to have little impact upon the WVTR performance of the bilayer films. However, by doubling this energy to 6 keV/TEOS molecule, a one order of magnitude improvement in performance of the bilayers with respect to the single layers can be observed. This performance enhancement continues with increasing input energy up to ~25 keV/TEOS molecule, where the difference in the encapsulation performance of films with and without a buffer layer is essentially three orders of magnitude. The importance of the porous buffer layer in the bilayer architecture with respect to achieving an exceptionally low overall effective WVTR is therefore clearly highlighted.
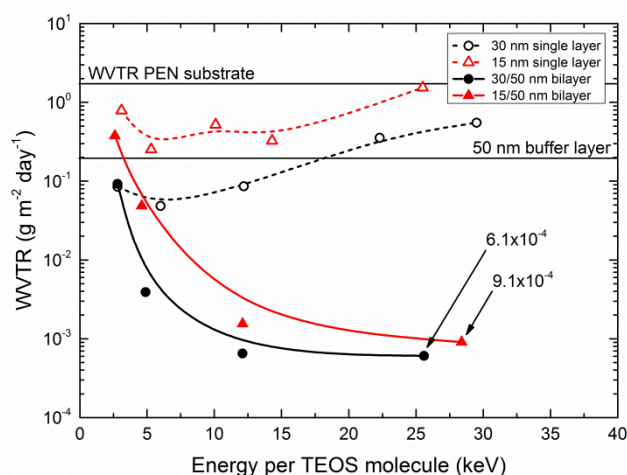
Figure 1. Effective WVTR (at 40°C, 90% RH) with respect to increasing input energy per TEOS molecule for synthesis of the barrier layer [26].

As expected, due to the thickness of the barrier layers, both single and bilayer films with 30 nm barriers consistently outperform films with 15 nm barriers deposited at equivalent deposition input energies. Nonetheless, the difference in the encapsulation performance between the two bilayer films decreases as the deposition input energy increases due to gradually intensified processing conditions (increased plasma residence time in conjunction with decreased precursor flux), which are likely to result in the formation of performance limiting macro-defects [26]. This trend is not observed for the single layer films, probably because the difference in the total film thickness still carries a more prominent role.

Interestingly, the encapsulation performance of the single layer barrier films initially improves with increasing input energy per TEOS molecule, but progressively deteriorates after 6 keV/TEOS molecule. The 15 nm single layer film deposited at 25 keV/TEOS molecule in fact exhibits essentially no encapsulating ability at all. As the decline in performance occurs for both the 30 nm and 15 nm single layer films, a similar phenomenon is likely responsible. It is known from attenuated total reflectance-Fourier transform infrared (ATR-FTIR) analysis of barrier films that the intrinsic porosity gradually decreases with increasing input energy/TEOS molecule, as the concentration of silica network-disrupting silanol groups (Si–OH) decreases thus increasing the film lattice density as a consequence [26]. Therefore it is likely that after 6 keV/TEOS molecule, the effective WVTR increases for the single layer films due to the gradual appearance of macro-defects, rather than the intrinsic or lattice porosity of the silica-like network increasing [30]. As aforementioned, it is speculated that macro-defects can result from gradually intensified processing conditions, namely the increased plasma residence times and decreased precursor flow rates required to attain the desired increases in input energy per TEOS molecule necessary for dense intrinsic barrier layer synthesis. Both increased plasma residence time and decreased precursor flux can in turn influence the film growth mechanism, possibly stimulating 'island' growth as opposed to layer-by-layer growth [33–37], and increase plasma-surface(polymer) interactions, inducing processes such as etching [38–40],

Together these events could therefore lead to macro-defect formation, most likely observed to a significantly greater extent in the absence of a buffer layer.

In order to determine if macro-defects, or pinholes, were indeed present and therefore responsible for the very poor encapsulation performance of the single layer barriers, solvent vapour exposure analysis was performed on the 30 nm single and bilayer films. As can be seen in Figures 2 and 3, the number and density of pinholes in the 30 nm single layer barrier films increases as a function of increasing input energy per TEOS molecule during the deposition process, and also consequently, increasing plasma residence time and decreasing precursor flux. These pinholes are with considerable certainty, the main reason for the very poor encapsulation performance observed for the high input E/TEOS buffer-less films, as it is known from ATR-FTIR analysis that increasing the input E/TEOS during the barrier layer deposition decreases the intrinsic porosity of the films [26]. A transition occurs for single layer films deposited from 6 – 12 keV/TEOS, where the effective WVTR converts from being controlled by the intrinsic film porosity to being dominated by the macro-defects. It is known that the intrinsic porosity of the 12.2 keV/TEOS film is less than that for the 6.0 keV/TEOS film [26], however the density of macro-defects increases to such an extent that the lower intrinsic porosity of the 12.2 keV/TEOS film has little or no influence on the WVTR, resulting therefore in a poorer encapsulation performance.
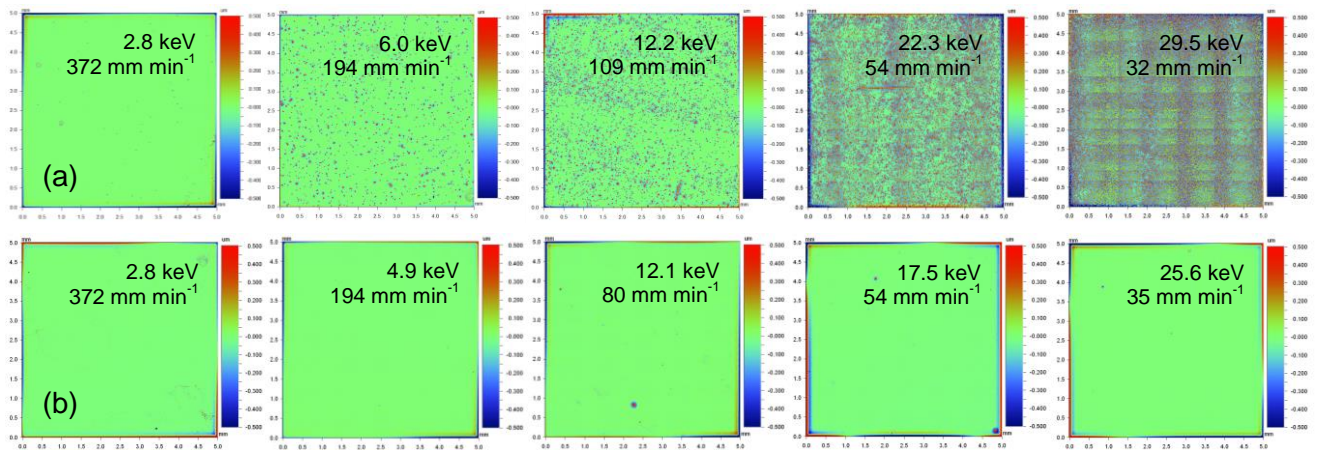

Figure 2. Interferometric micrographs illustrating the outcome of solvent vapour exposure analysis carried out on: (a) 30 nm single layer and (b) 30/50 nm bilayer films deposited at a range of deposition input energies and foil transport speeds. Small high features are indicative of blister formation resulting from the presence of macro-defects such as pinholes. The distance between two defect regions for the 22.3 and 29.5 keV samples are approx. 2 mm and 1 mm respectively.

Also observed in the 30 nm single layer interferometric micrographs are linear regions of higher defect density, particularly obvious in the 22.3 keV/TEOS and 29.5 keV/TEOS samples. Equally apparent are thin scratches oriented in the direction of foil transport. The regions of higher defect density are therefore aligned perpendicular to the foil transport and thus parallel with the plasma discharge. It is likely that a 'stick- slip' mechanism occurs during the substrate transport, especially at lower foil transport speeds (and hence increased E/TEOS), and consequently certain areas of the film remain in the plasma discharge for longer time intervals than others. This is supported by a direct correlation relating the distance between two defect regions and the foil transport speed for the 22.3 and 29.5 keV/TEOS samples (Figure 2). Hence this would infer that an increased plasma residence time does result in the formation of macro-defects in the single layer films.
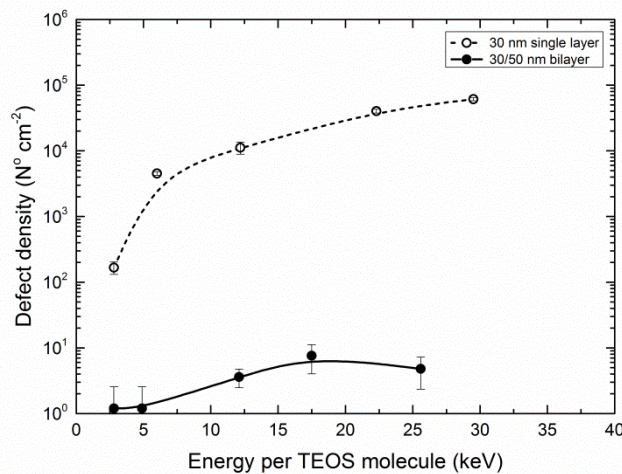
Figure 3. Defect density data obtained from interferometric micrographs (Figure 2) plotted as a function of increasing input energy per TEOS molecule for the synthesis of the barrier layer.

Moreover, as only very few defects were observed in the equivalent high deposition energy 30 nm barrier samples incorporating a buffer layer, the results displayed in Figures 2 and 3 indicate that the macro-defects form primarily in the absence of said buffer layer. The function of the buffer layer therefore likely includes the prevention of defect-inducing plasma-surface interactions, as outlined above.

AFM micrographs displayed in Figure 4 illustrate the typical surface morphologies of the PEN substrate, the single layer barriers, the buffer layer and the bilayer barriers. It is fairly evident that the morphology of all the deposited layers follows that of the PEN substrate, with the 15 nm high energy single layer being the only exception. Small, high features can be seen in the low energy 30 nm single layers, the buffer layer and all bilayer films, but disappear for the high energy 30 nm single layers and all 15 nm single layers. It still remains unclear what causes the formation of these small high features, however, their disappearance correlates with an increase in the WVTR and also the presence of macro-defects.
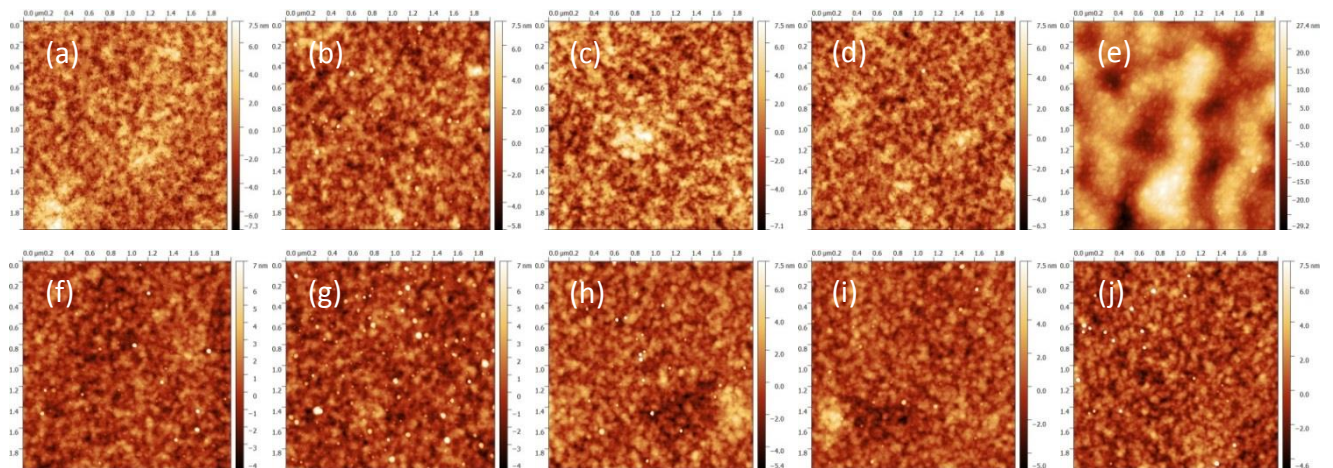

Figure 4. AFM micrographs illustrating the surface morphology of: (a) the PEN substrate; (b) the 30 nm single layer barrier deposited at 6.0 keV/TEOS molecule; (c) the 30 nm single layer barrier deposited at 29.5 keV/TEOS molecule; (d) the 15 nm single layer barrier deposited at 5.3 keV/TEOS molecule; (e) the 15 nm single layer barrier deposited at 25.5 keV/TEOS molecule; (f) the buffer layer; (g) the 30 nm bilayer barrier deposited at 4.9 keV/TEOS molecule; (h) the 30 nm bilayer barrier deposited at 25.6 keV/TEOS molecule; (i) the 15 nm

bilayer barrier deposited at 4.6 keV/TEOS molecule and (j) the 15 nm bilayer barrier deposited at 28.4 keV/TEOS molecule.

The 15 nm single layer film deposited at the highest E/TEOS shows a remarkably different morphology to that of the other films. It is also comparatively very rough, with an RMS roughness of 11.3 ± 2.9 nm (Figure 5) and adheres exceptionally poorly to the PEN substrate. It is therefore likely that the deposition parameters for the synthesis of this layer, namely the very low precursor flux in combination with a relatively high plasma residence time and the absence of a buffer layer, are not suitable for barrier film synthesis. This is verified by the essentially non-existent encapsulation performance shown in Figure 1. In this particular case it is possible that the presence of a 'semi-porous' buffer layer would act not only to prevent defect-inducing plasma-surface interactions, but also to mechanically stabilize the porous PEN substrate in preparation for the deposition of the extremely thin, dense silica barrier layer. The buffer layer may function as a bridging material to reduce the high initial structural stress felt ordinarily by the two layers of differing density, thus preventing crack formation and delamination [29], of the barrier layer.

Figure 5 shows the data obtained from the topographic analysis of the AFM images illustrated in Figure 4. An increase in RMS roughness as a function of increasing input energy per TEOS molecule during the deposition process can be observed for both single and bilayer films, however the extent of said increase and the starting point is both much steeper and higher for the single layer films. The thickness of the barrier layers, however, appears to have little or no impact upon the RMS roughness values calculated, suggesting the underlying materials (the PEN substrate in the case of the single layers, and the silica buffer layer in the case of the bilayers) pose a greater influence.
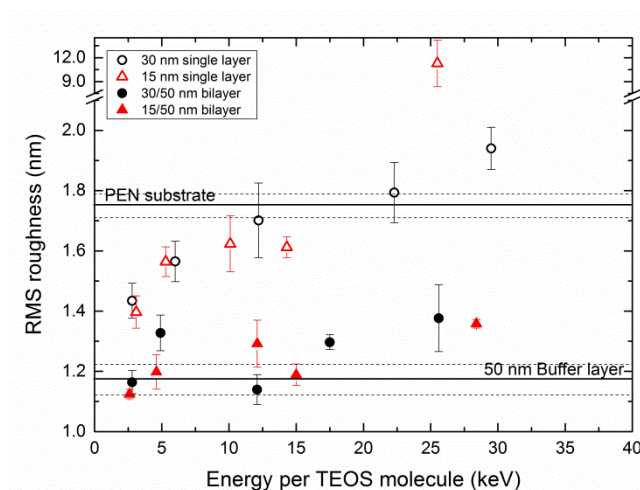

Figure 5. Topographic data obtained from AFM micrographs (Figure 4) RMS roughness plotted as a function of increasing input energy per TEOS molecule for the synthesis of the barrier layer.

All bilayer films are seen to have RMS roughness values less than 1.4 nm. This RMS roughness value is considerably less than the PEN substrate that has an RMS roughness of 1.75 ± 0.04 nm. It is evident that the presence of a buffer layer is responsible for the decreased RMS roughness of the bilayer films, as it appears to smooth the PEN substrate in preparation for the barrier layer deposition.

A direct correlation can be observed between the encapsulation performance, the number of macro-defects in the single 30 nm layers (Figures 1, 2 and 3) and the corresponding RMS roughness. As stated previously, an increase in E/TEOS combines increased plasma residence time with decreased precursor flows and hence film growth rate. This therefore results in intensified plasma-surface(polymer) interactions (such as etching) that could contribute to the rapid increase in RMS roughness observed for the single layer films [38–40]. As before, regarding the formation of macro-

defects, the presence of a buffer layer limits the extent of said plasma- surface(polymer) interactions thus reducing the RMS roughness of the bilayers, despite equivalent barrier deposition conditions. The primary function of the buffer layer, rather than to merely smoothen the PEN substrate, could in fact be as a protection layer to prevent excessive plasma-surface interactions during the barrier layer deposition in harsh processing conditions.

4. Conclusions
The function of the porous buffer layer in flexible bilayer silica-like encapsulation films deposited using the industrially and commercially relevant roll-to-roll AP-PECVD process was evaluated. Extensive effective WVTR measurements confirmed that the presence of this buffer layer within the bilayer architecture was mandatory in order to achieve excellent encapsulation performances as low as 6.1×10^{-4} g m^{-2} day^{-1} (at 40°C, 90% RH), capable of protecting flexible photovoltaics and thin film transistors from oxygen and water degradation. The buffer layer was found to prevent the formation of macro-defects in the bilayer architecture, which otherwise occurred when identical barrier layers were deposited directly onto the flexible PEN substrate. It is speculated from solvent vapour exposure analysis and AFM measurements that the buffer layer acted as a protective coating to prevent excessive plasma-surface interactions, which are likely to occur as a result of the harsh processing conditions (increased plasma residence time in conjunction with decreased precursor flux) required for the deposition of dense barrier layers. For the continued development of AP-PECVD processing of silica-like thin films designed for the encapsulation of flexible electronics, the use of a porous buffer layer in the thin film architecture is therefore essential.

References
[1]   Han Y C, Kim E, Kim W, Im H-G, Bae B-S and Choi K C 2013 *Org Electron.* **14** 1435–40

[2]   Park J-S, Chae H, Chung H K and Lee S I 2011 *Semicond Sci Technol.* **26** 034001

[3]   Morlier A, Cros S, Garandet J P and Alberola N 2013 *Sol Energy Mater Sol Cells* **115** 93–9

[4]   Lewis J 2006 *Mater Today* **9** 38–45

[5]   Weaver M S *et al* 2002 *Appl Phys Lett.* **81** 2929–31

[6]   Graff G L, Williford R E and Burrows P E 2004 *J Appl Phys.* **96** 1840–9

[7]   Seo S-W, Jung E, Lim C, Chae H and Cho S M 2012 *Thin Solid Films* **520** 6690–4

[8]   Burrows P E *et al* 2001 *Proc SPIE* **4105** 75–83

[9]   Starostin S A, Creatore M, Bouwstra J B, van de Sanden M C M and de Vries H W 2015 *Plasma Process Polym.* **12** 545–54

[10]   Majee S, Geffroy B, Bonnassieux Y and Bourée J E 2014 *Surf Coatings Technol.* **254** 429–32

[11] Majee S, Cerqueira M F, Tondelier D, Geffroy B, Bonnassieux Y, Alpuim P and Bourée J E 2015 *Prog Org Coatings* **80** 27–32

[12] Nagai S 2015 *Surf Coatings Technol*. **267** 59–64

[13] Dameron A A, Davidson S D, Burton B B, Carcia P F, McLean R S and George SM 2008 *J Phys Chem C* **112** 4573–80

[14] Ali K, Choi K-H, Jo J and Lee YW 2014 *Mater Lett*. **136** 90–4

[15] Hoffmann L, Theirich D, Hasselmann T, Räupke A, Schlamm D and Riedl T 2016 *J Vac Sci Technol A Vacuum, Surfaces, Film.* **34** 01A114

[16] Langereis E, Creatore M, Heil S B S, van de Sanden M C M and Kessels W M M 2006 *Appl Phys Lett*. **89** 081915.

[17] Starostin S A, Keuning W, Schalken J-P, Creatore M, Kessels W M M, Bouwstra J B, van de Sanden M C M and de Vries H W 2016 *Plasma Process Polym*. **13** 311–5

[18] Alpuim P, Majee S, Cerqueira M F, Tondelier D, Geffroy B, Bonnassieux Y and Bourée J E 2015 *Thin Solid Films* **595** 258–65

[19] Chen T N, Wuu D S, Wu C C, Chiang C C, Lin H B, Chen Y P and Horng R H 2006 *Thin Solid Films* **514** 188–192

[20] Majee S, Cerqueira M F, Tondelier D, Geffroy B, Bonnassieux Y, Alpuim P and Bourée J E 2013 *Surf Coatings Technol*. **235** 361–6

[21] Zhang S, Xue W and Yu Z 2015 *Thin Solid Films* **580** 101–5

[22] Majee S, Cerqueira MF, Tondelier D, Vanel J C, Geffroy B, Bonnassieux Y, Alpuim P and Bourée J E 2015 *Thin Solid Films* **575** 72–5

[23] van Assche F J H, Unnikrishnan S, Michels J J, van Mol A M B,van de Weijer P, van de Sanden M C M and Creatore M 2014 *Thin Solid Films* **558** 54–61

[24] da Silva Sobrinho A S, Czeremuszkin G, Latrèche M and Wertheimer M R 2000 *J Vac Sci Technol A Vacuum, Surfaces, Film* **18** 149–57

[25] Aresta G, Premkumar P A, Starostin S A, de Vries H, van de Sanden M C M and Creatore M 2010 *Plasma Process Polym*. **7** 766–74

[26] Elam F M, Starostin S A, Meshkova A S, van der Velden-Schuermans B C A M, Bouwstra J B, van de Sanden M C M and de Vries H W 2016 Atmospheric pressure roll-to-roll plasma enhanced CVD of high quality silica-like bilayer encapsulation films. *Plasma Process Polym*. doi:10.1002/ppap.201600143

[27] Petersen J, Bardon J, Dinia A, Ruch D and Gherardi N 2012 *Appl Mater Interfaces* **4** 5842–82

[28] Kim N, Potscavage W J, Sundaramoothi A, Henderson C, Kippelen B and Graham S 2012 *Sol Energy Mater Sol Cells* **101** 140–6

[29] Deilmann M 2008 Silicon oxide permeation barrier coating and sterilization of PET bottles by pulsed low-pressure microwave plasmas PhD thesis Ruhr-Universitat Bochum

[30] Roberts A P, Henry B M, Sutton A P, Grovenor C R M, Briggs G A D, Miyamoto T, Kano M, Tsukahara Y and Yanaka M 2002 *J Memb Sci*. **208** 75–88

[31]   Shamiryan D, Baklanov M R and Maex K 2003 *J Vac Sci Technol B* **21** 220–6

[32]   Necas D and Klapetek P 2012 *Cent Eur J Phys*. **10** 181–8

[33]   Teshima K, Inoue Y, Sugimura H and Takai O 2002 *Thin Solid Films* **420-421** 324–9

[34]   Teshima K, Inoue Y, Sugimura H and Takai O 2003 *Surf Coatings Technol*. **169-170** 583–6

[35]   Dudeck D, Yanguas-Gil A, Yubero F, Cotrino J, Espinos J P, de la Cruz W and Gonzalez-Elipe A R 2007 *Surf Sci*. **601** 2223–31

[36]   Dennler G, Houdayer A, Ségui Y and Wertheimer M R 2001 *J Vac Sci Technol A Vacuum, Surfaces, Film*. **19** 2320–7

[37]   Dennler G, Houdayer A, Latrèche M, Ségui Y and Wertheimer M R 2001 *Thin Solid Films*. **382** 1–3

[38]   Fang Z, Wang X, Shao R, Qiu Y and Edmund K 2011 *J Electrostat*. **69** 60–6

[39]   Zhang C, Shao T, Long K, Yu Y, Wang J, Zhang D, Yan P and Zhou Y 2010 *IEEE Trans Plasma Sci*. **38** 1517–26

[40]   Fang Z, Yang H and Qiu Y 2010 *IEEE Trans Plasma Sci*. **38** 1615–23